Applied Materials Today 12 (2018) 389–401

Contents lists available at ScienceDirect

Applied Materials Today

journal homepage: www.elsevier.com/locate/apmt

Investigation into the toxic effects of graphene nanopores on lung cancer cells and biological tissues

Tanveer A. Tabish[a,*], Md Zahidul I. Pranjol[b,c], F. Jabeen[d], Trefa Abdullah[b], Asif Latif[d], Adeel Khalid[d], M. Ali[d], Hasan Hayat[a], Paul G. Winyard[b], Jacqueline L. Whatmore[b,*], Shaowei Zhang[a,*]

[a] Centre for Graphene Science, University of Exeter, Exeter EX4 4QL, United Kingdom
[b] Institute of Biomedical and Clinical Science, University of Exeter Medical School, St Luke's Campus, EX1 2LU, United Kingdom
[c] William Harvey Research Institute, Queen Mary University of London, London EC1M 6BQ, United Kingdom
[d] Department of Zoology, Government College University, Faisalabad 38000, Pakistan

ARTICLE INFO

Article history:
Received 6 June 2018
Received in revised form 6 July 2018
Accepted 11 July 2018

Keywords:
Graphene nanopores
Cytotoxicity
In vivo test
In vitro test
Intraperitoneal administration
Biocompatibility

ABSTRACT

As an inexpensive monolayer archetypal member of the carbon family, graphene has triggered a new 'gold rush' in nanotechnology for achieving unique properties that were not available in many traditional materials. Owing to these unique features, graphene-related materials are finding new uses in nanomedicine and synthetic biology in addition to their diverse applications in electronics, optoelectronics, photonics and environmental clean-up. The increased production of graphene nanostructures and increased likelihood of exposures to these substances in environmental and occupational settings has raised concerns about adverse health outcomes. In particular, the biological effects of these materials need to be assessed to ensure risk free, sustainable development of graphene for widespread applications. In this work, for the first time, we studied the *in vitro* and *in vivo* interactions of a relatively new derivative of graphene, graphene nanopores (GNPs) in mammalian systems, to systematically elucidate the possible mechanism of their toxicity over time. This study showed that GNPs induced early apoptosis in both SKMES-1 and A549 lung cancer cells. However, late apoptosis is only induced at concentrations higher than 250 μg/ml, suggesting that, although GNPs at lower concentrations induce upregulation of phosphatidylserine on the cell surface membrane (i.e. early apoptotic event), GNPs do not significantly disintegrate the cell membrane. We also showed that rats intraperitoneally injected with GNPs suffered sub-chronic toxicity in a period of 27 days when tested at single and multiple doses of GNPs (5 and 15 mg/kg) as evidenced by blood biochemistry, organo-somatic index, liver and kidney enzymes functions analysis, oxidative stress biomarkers and histological examinations. In sum, our results show that GNPs are likely to have a low bioavailability in SKMES-1 and A549 lung cancer cells and rats. Nevertheless, this must be considered against the context of a wider lack of knowledge regarding the bioavailability, fate and behaviour of this type of new porous framework of graphene in natural systems. Therefore, a more long-term GNPs exposure regime, more relevant to real-life environmental consequences, is needed to fully determine the transport capacities of GNPs in living systems.

1. Introduction

Graphene has become a 'superstar' in nanomedicine with applications to improve diagnostics, therapeutics, and genetic risk factors, owing to its multifaceted properties such as small size, large surface area-to-volume ratio, quantum size effects, and unique physicochemical properties [1–3]. One important advantage of graphene-based materials is their ability to effectively cross biological barriers such as the blood brain barrier, highlighting their potential as a drug delivery vehicle for anticancer therapeutic agents. In particular, the combined enhanced permeability and retention effect would facilitate their accumulation in tumours, releasing therapeutic levels of drugs into the target cells with reduced side effects [4]. Typically, graphene quantum dots have many properties far superior to conventional quantum dots such as photoluminescence, low toxicity and interplay between size and optical features which have been utilized as diagnostic imagining tools as well as photodynamic/photothermal therapy [5]. Similar use of three-dimensional graphene foam for stem cell therapy of

* Corresponding authors.
E-mail addresses: tt302@exeter.ac.uk (T.A. Tabish), J.L.Whatmore@exeter.ac.uk (J.L. Whatmore), s.zhang@exeter.ac.uk (S. Zhang).

https://doi.org/10.1016/j.apmt.2018.07.005

stroke and its bioconjugates in regenerative medicine has been described in recent literature [6]. Recently, graphene nanopores (GNPs) have also been used in applications such as DNA sequencing [7–9] and water treatment [10,11] and GNPs have provided unique porous frameworks [12]. Porous graphene biointerfaces have also recently been reported as an effective antimicrobial agents with highly efficiently bactericidal activities against both Gram positive and Gram negative bacteria [13,14]. Matharu et al. [15] have reported the effects of graphene nanoplatelet-loaded polymer fibres on microbial growth of two Gram negative bacteria *Escherichia coli* and *Pseudomonas aeruginosa*. They determined the minimum inhibitory concentration of graphene-fibre which in turn can produce the highest antibacterial effects while remaining non-toxic to the normal cells. This study revealed that 8 wt% of graphene-fibres showed good antibacterial effects owing to the direct contact between bacterial cells and the sharp edges of the graphene nanostructures. This direct contact is also responsible for severe membrane deformation and the efflux of cytoplasmic material [16]. One drawback of the use of GNP's is that very few synthesis techniques are available. However, techniques such as electron beam irradiation, ion bombardment, doping, templating, chemical etching, chemical vapour deposition and other chemical methods have now been utilized for their preparation [9,17–20]. The drawbacks of these methods are the low production yield and the problems associated with their separation/purification. To address this omission, we have recently reported a study demonstrating a novel and facile approach to GNPs synthesis via thermal treatment of reduced graphene oxide without using any catalyst or template-based approach [21].

GNP, a thin, flexible material with excellent electrical addressability and robust mechanical properties is promising for label-free protein detection, DNA sequencing and high throughput wastewater based-micropollutant decontamination [7–11]. The high specific surface area and nanoporous framework allows direct sensing and sequencing of atomic-scale biomolecules. In recent years, cellular internalization and trans-barrier transport of micro/mesoporous graphene nanosheets have been the subject of major developments in nanobiotechnology. It is evident that nanoscale materials with a diameter less than 100 nm can enter cells, while nanoparticles smaller than 40 nm in diameter can reach the cellular nuclei. Particles with diameters below 35 nm are able to reach the brain by passing through the blood–brain barrier [22–24], while larger nanoparticles are excluded which in turn reduces the delivery of theranostic nanoparticles [25–27]. A better understating of the physiochemical properties of graphene, the interaction between graphene and cells, and possible toxicity mechanisms is of critical importance to outline potential biomedical applications of these materials. The proposed mechanism of GNPs toxicity is depicted in Fig. 1. The widespread use of graphene-based materials and their potential toxic effects are likely to exacerbate several health concerns [26,27]. Most laboratory experiments investigating the potential applications of GNPs in life sciences have not considered the toxicity associated with GNPs in their testing regimes. Recently, however, a few studies have examined the *in vitro* and *in vivo* toxic implications of three dimensional graphene foam to investigate the bioavailability and subsequent toxicity potential [28,29]. The pre-clinical risks, adverse effects of GNPs exposure, and approaches to minimize their health hazards still remain undefined. However, inhalation of graphene structures is believed to be a risk factor for cardiorespiratory disease. For example, inhaled graphene nanoplatelets can be transported deep within the distal regions of the lungs and trigger chronic inflammation in the respiratory tract [30]. It is generally thought that the placenta, lung, gastrointestinal tract and skin act as major barriers for many nanostructures entry into living organisms [31]. Indeed, a recent study on mice demonstrated that intratracheally delivered few-layered

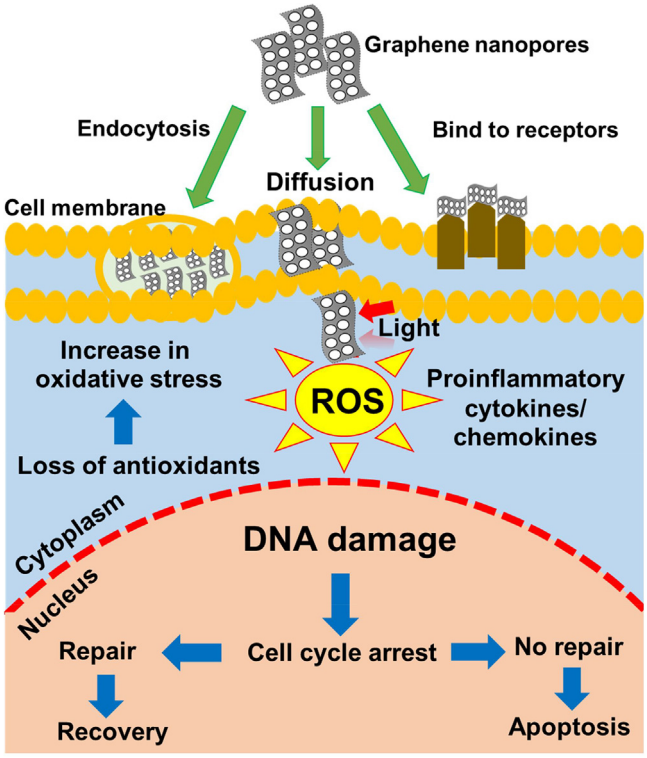

Fig. 1. Schematic illustration of the potential mechanisms of action of graphene nanopores (GNPs). When graphene nanopores reach the exterior membrane of a cell, they interact with the plasma membrane or extra-cellular matrix and enter the cell, mainly through diffusion, endocytosis and/or binding to receptors. The potential toxic effects of graphene mainly depend on its physicochemical characteristics, the nature of its interaction with cells and its accumulation in specific organs. Upon interaction with light, graphene can generate reactive oxygen species, which in turn can cause oxidative stress, loss in cell functionality, pro-inflammatory responses and mitochondrial damage. Uptake of graphene into the nucleus may cause DNA-strand breaks and induction of gene expression via the activation of transcription factors, cell death and genotoxicity.

graphene was mainly retained in the lung, with 47% remaining after 4 weeks and this resulted dose-dependent acute lung injury and pulmonary oedema [32]. An *in vitro* study of the effects of graphene and graphene oxide on human skin HaCaT keratinocytes demonstrated that oxidized graphene was the most cytotoxic, inducing mitochondrial and plasma-membrane damage, and suggesting low cytotoxic effects at the skin level [33]. Reduced graphene oxide is more toxic than graphene oxide as evidenced by many studies reported recently [34,35]. This is primarily due to its sharp edges and structural morphology. In contrast to the typically soluble nanoparticles examined in conventional toxicology investigations, graphene nanostructures have different shapes and surface areas, and which in turn can significantly influence their diffusion, dispersion, aggregation and agglomeration in plasma. Importantly, these "tunable" characteristics of graphene account for the varying toxic outcomes on the tissues. *In vivo, following* toxicity testing of graphene, post-mortem histological examinations of liver alterations have revealed hypertrophy of hepatocytes, necrosis and inflammatory cell infiltration in liver and kidney tissues [36]. The level of organ function and oxidative stress has been reported to affect the fate, transport and toxicity of graphene in organs but there is currently a lack of consistency in this regard [36]. Liver enzyme functions can be used to reveal the biodistribution, metabolism, and excretion patterns of graphene. Similarly, investigation of oxidative stress indicators is a commonly acknowledged mechanism adopted to investigate cellular injuries in mammals. Antioxidants act as a defence system to reinstate the cellular redox

balance when oxidative stress is generated as a result of excess production of reactive oxygen species. Disruption of this critical balance in the presence of excessive reactive oxygen species triggers the activation and promotion of a pro-inflammatory cascade, which in turn may cause mitochondrial release of proapoptotic factors potentially leading to cell death. Hepatocytes are key targets for reactive oxygen species damage, and therefore liver function and biomarkers of oxidative stresses should be investigated with great care.

Lung cancer cell lines are commonly used to assess the cytotoxicity of an experimental material for biomedical applications. Cancer cell lines such as lung and breast were selected by National Cancer Institute as models to screen drugs/compounds as a prelude to testing in xenografts or animal models [37]. Use of human cell lines in toxicity assays allows us to selectively test mechanisms of cell toxicity in a controlled environment, which can be very difficult, time consuming and laborious to carry out in rat models. Also, animal models are genetically very different than human. Bioavailability experiment with animal models cannot explain the cellular and molecular mechanisms of interactions between cell membrane or cellular organelles and the tested compounds, which can only be achieved using well-defined and well-characterised human cell lines such as lung, breast cancer cells. Isolating primary human cell for each organ for *in vitro* study is not cost-effective and it also may produce huge variability due to significant heterogeneity among humans on genomic, proteomic and phenotypic levels. Human cancer cell lines hold genetic information that is well-characterised and translatable to human studies. Also, using human cancer cell lines to test for *in vitro* toxicity give us an indication of the range of doses that can be applied in animal models. *In vivo*, the efficacy of the treatments remains non-selective, non-specific and is carried out in an uncontrolled environment (e.g. genetically heterogeneous mice). Thus, we utilized human cell lines *in vitro* to carry out our preliminary toxicity experiments in a controlled, 2D environment which was then repeated in *in vivo* models to better understand the effect of the compound in a 3D, uncontrolled environment. We studied two types of lung cancer cells (e.g. adenocarcinoma and squamous cell carcinoma- both of epithelial origin) for two reasons: (a) cancer cells evolve to evade the immune system and display resistance to a number of therapeutic responses such as chemotherapy and radiotherapy, and hence possess a therapeutic challenge. Due to the occupational exposure of such graphene-based nanomaterials, it is highly likely that these nanomaterials can be inhaled in humans which may lead to respiratory pathology. Thus, testing toxic effects of this nanoparticle in lung cancer cell lines was advantageous over using somatic cell lines; and (b) unlimited proliferation is a predominant feature of all cancer cell lines compared to the limited proliferative capacity of somatic cells. During passaging, somatic cells undergo anoikis when they detach from the extracellular matrix coating, resulting in a decreased number of cells in the next passage. Consequently, the resultant cell death due to the testing compound may not be a true representation of the toxicity of a compound. Also, as the passage number increases, somatic cells may become less responsive to an exogenous therapeutic assault. These phenomena are rarely observed or are absent in cancer cells.

Clearly, *in vitro* and *in vivo* investigations into the toxicity of graphene nanostructures is becoming increasingly important. In response to this, the present study investigates the toxic effects of GNPs on lung cancer cells (SKMES-1 and A549) *in vitro* and in rats *in vivo*, specifically, biochemical, serum enzyme analyses, complete blood count as well as histological analysis have been used in this study.

2. Results

2.1. In vitro *toxic effects of GNPs on lung cancer cells*

Representative FACS images and analysis of one experiment of cell viability have been shown in Fig. 2. Fig. 3A demonstrates that after 24-h exposure to GNPs, the cell viability of A549 cells exhibited a significant dose-dependent reduction from 50 to 500 μg/ml. For example, after 24 h reduction in the percentage of living cell were 52.8%, 42.5% and 33.2% at concentrations 50, 250 and 500 μg/ml

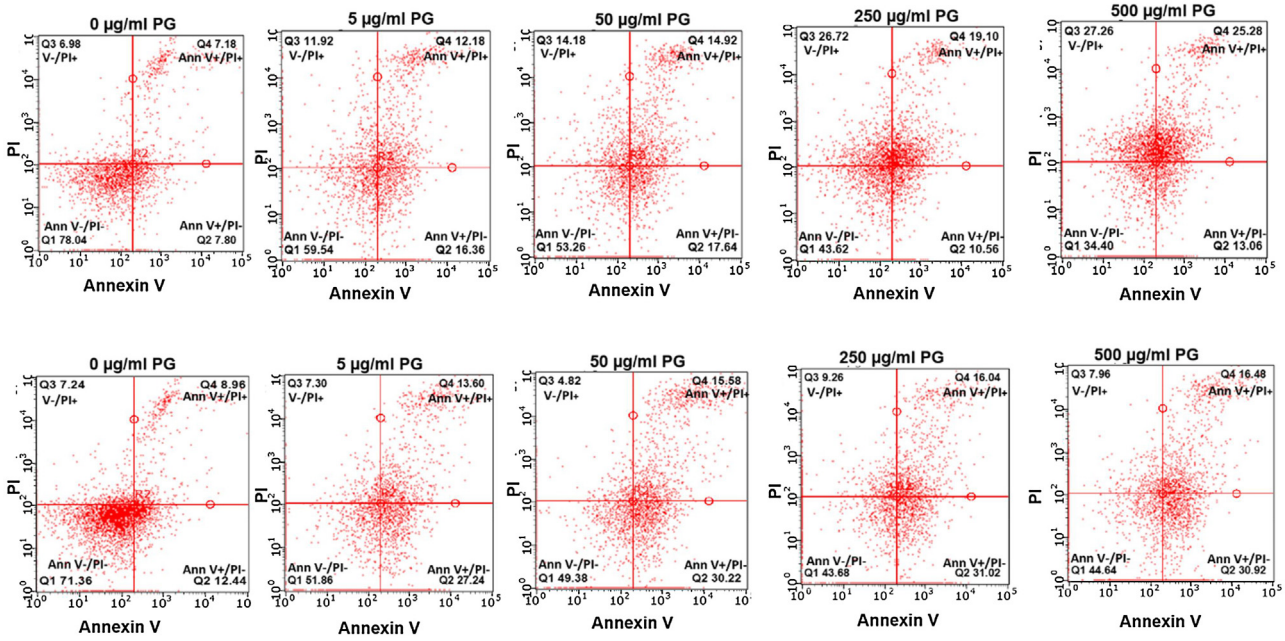

Fig. 2. Representative fluorescence-activated cell sorting (FACS) analysis of cell viability, early apoptotic, late apoptotic, and necrotic cells of selected concentrations of graphene nanopores (GNPs) in two different lung cancer cell lines (A549 and SKMES-1). Data are presented as percentage of the cell population. Cell viability of A549 (upper panel) and SKMES-1 (lower panel) is shown at selected concentrations. Experiments were performed and interpreted as follows: annexin V^{-ve}/PI^{-ve} cells (lower left quadrant), annexin V^{+ve}/PI^{-ve} cells (lower right quadrant), annexin V^{+ve}/PI^{+ve} (upper right quadrant) and annexin V^{-ve}/PI^{+ve} (upper left quadrant) were considered as living, early apoptotic, late apoptotic, and necrotic cells.

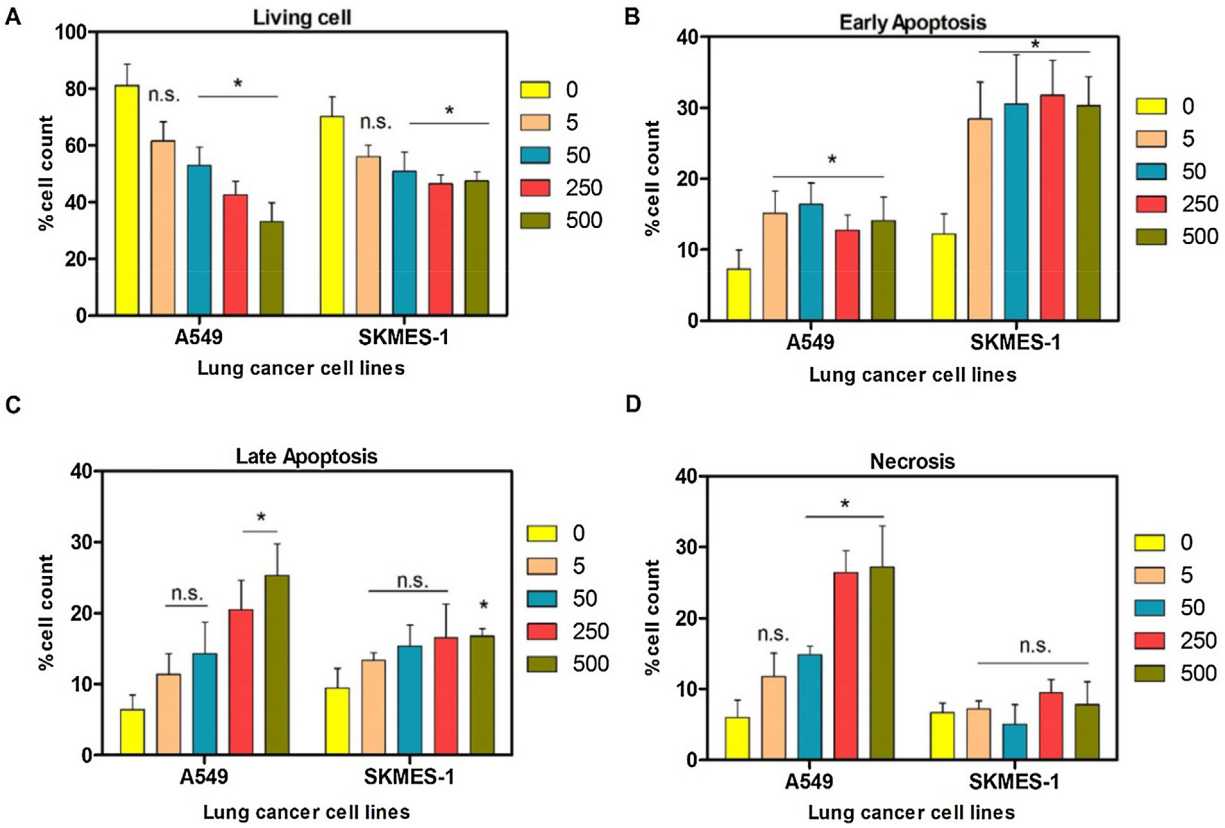

Fig. 3. Bar graph quantifying the percentage of dead, living, early-stage apoptotic, and late-stage apoptotic cells in response to different concentrations of porous graphene (GNPS). Flow cytometry analysis of A549 and SKMES-1 lung carcinoma cells stained with annexin V (apoptosis) and propidium iodide (PI; late apoptosis and necrosis) following 24 h of treatment with varying concentrations of GNPs (0–500 μg/ml). (A) graphic representation of percentage of living cells (B) early apoptosis (C) late apoptosis, (D) necrosis in response to GNPs. Data are represented as mean ± SD of three independent experiments. $^{*}p < 0.05$ vs control. n.s. denotes not significant.

respectively, compared to control (0 μg/ml, ~80%). A similar observation was made in SKMES-1 cells where GNPs concentrations 50 and above induced significant reduction of living cells. However, the reduction was not dose dependent (Fig. 3A). For example, at 50, 250 and 500 μg/ml of GNPs, percentage count for living cells were 50.8%, 46.5% and 47.4% respectively, compared to control (0 μg/ml, 70%). The number of cells undergoing early apoptosis significantly increased in a dose dependent manner following treatment with 5 μg to 500 μg/ml GNPs in both A549 and SKMES-1 cells (Fig. 3B). A dose-dependent increase in late apoptotic (Fig. 3C) and necrotic cells (Fig. 3D) was also observed in A549 cells, although no significant increase in necrosis was observed in the SKMES-1 cell line.

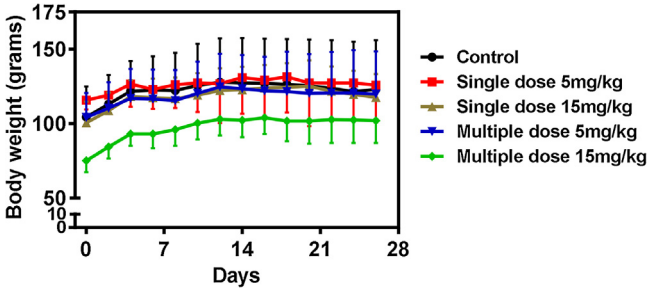

Fig. 4. Daily body weight (g) of control groups and treated groups of rats exposed to GNPs by intraperitoneal injection for 27 days. First dose was administered at day 0 for both single and multiple dose regimen, and the body weight was measured daily.

2.2. Effects of GNPs on body and relative organ weights

In vivo toxicity of GNPs was assessed in rats following 27-day repeated dose intraperitoneal injections. GNPs treatment did not affect the body weight of the treated rats during the 27-days exposure period for treatment with 5 mg/kg body weight either once or multiple doses (Fig. 4). No significant decrease in body weight was observed in rats administered GNPs up to 5 mg/kg. Rats in the high repeated dose group (15 mg/kg body weight) showed lower body weights after 27 days (Fig. 4) compared to the control group, but this did not reach significance. Organo-somatic indices demonstrated that organ weight did not change by the treatment of GNPs, compared to the control, supporting their low *in vivo* toxicity (Supplementary information Fig. 2).

2.3. Effects of GNPs on complete blood count in the rat

To examine the *in vivo* cytotoxicity of GNPs, we performed a complete blood count (CBC), liver and kidney function enzymes, biomarkers of oxidative stress and histological study of vital organs of control and treated rats. Treated animals received with either 5 or 15 mg GNPs/kg body weight as either a single dose or repeated doses (8 doses spread over a 27 day period). Toxic effects of GNPs on CBC were not observed (Fig. 5A–O) although there was a slight (6%) reduction in platelet numbers in the 15 mg/kg group (Fig. 5K). The proportion of lymphocytes remained stable (Fig. 5B) and total white cell count was unaffected (Fig. 5N).

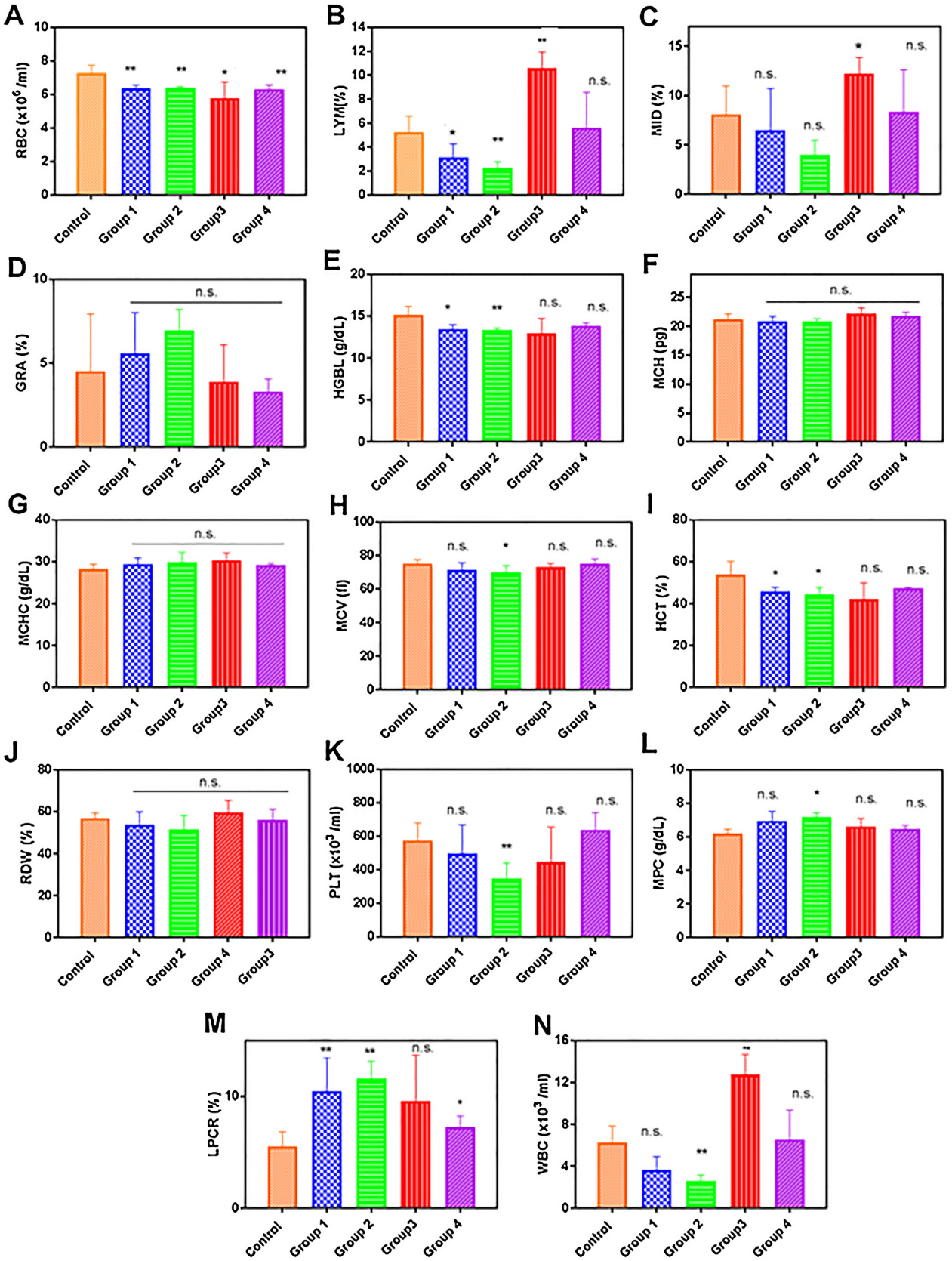

Fig. 5. (A–N) Complete blood count in rats after 27 days of GNPs administration. Rats ($n = 8$ per group) were intraperitoneally injected with single doses of 5 mg/kg body weight (group 1), 15 mg/kg body weight (group 2) or multiple doses of 5 mg/kg body weight (group 3) and 15 mg/kg body weight (group 4). Values are expressed as mean ± standard deviation, for: (A) red blood cell count (RBC); (B) lymphocytosis (LYM %); (C) mid-range absolute count (MID); (D) total % of granulocytes GRA; (E) haemoglobin (HBGL); (F) mean corpuscular haemoglobin (MCH); (G) mean corpuscular haemoglobin concentration (MCHC); (H) mean corpuscular volume (MCV); (I) hematocrit (HCT); (J) red cell distribution width (RDW); (K) platelet count (PLT); (L) mean platelet component (MPC); (M) large platelet concentration ratio (LPCR); and (N) white blood cell count (WBC). Data are represented as mean ± SD of three independent experiments. $^{*}p < 0.05$, $^{**}p < 0.01$ vs control. n.s. denotes not significant.

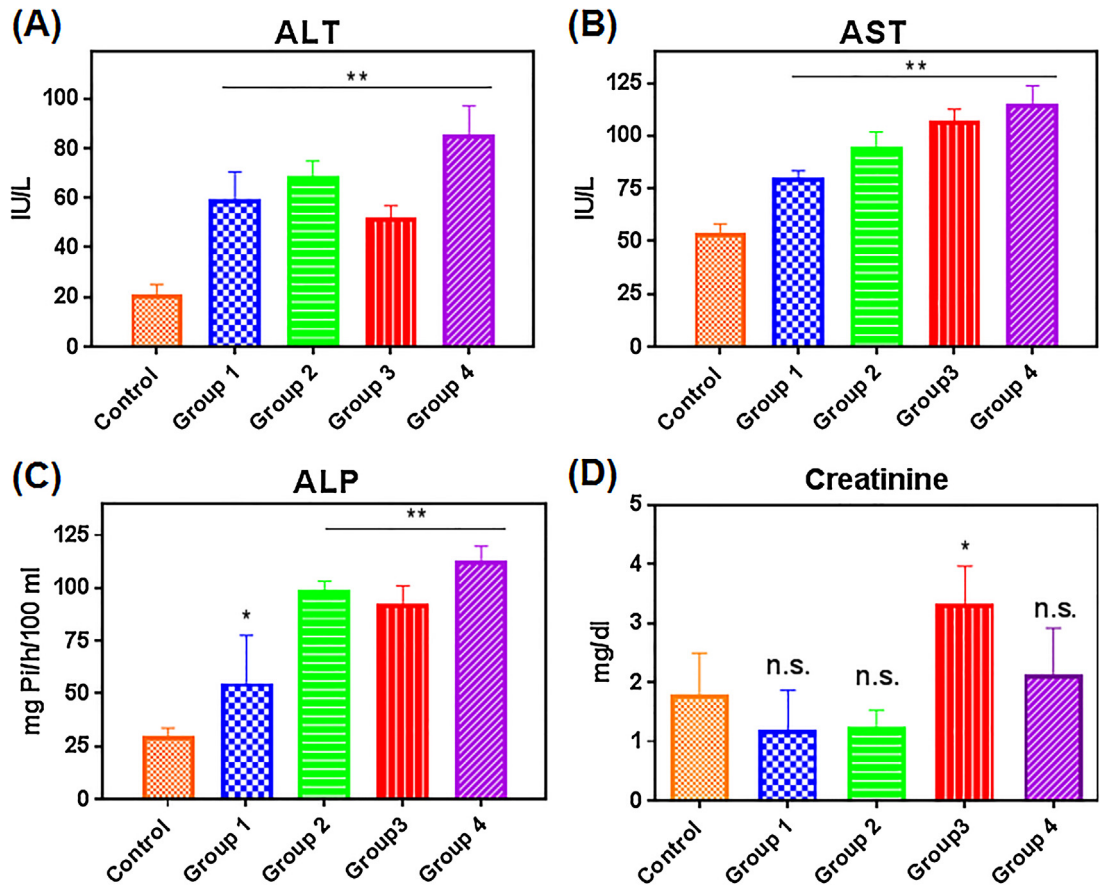

Fig. 6. Liver and kidney enzyme functions results in rats 27 days post GNPs administration. Rats ($n = 8$ per group) were intraperitoneally injected with single doses of 5 mg/kg body weight (group 1), 15 mg/kg body weight (group 2) or multiple doses of 5 mg/kg body weight (group 3) and 15 mg/kg body weight (group 4). Values are expressed as mean ± standard deviation, for: (A) alanine transaminase (ALT), (B) aspartate transaminase (AST), (C) alkaline phosphatase (ALP) and (D) creatinine. Data are represented as mean ± SD of three independent experiments. $^{*}p < 0.05$, $^{**}p < 0.01$ vs control. n.s. denotes not significant.

2.4. Liver and kidney function analysis

Alterations were observed in liver and kidney functions following GNPs treatment (Fig. 6) i.e., the results showed that the activities of ALT, AST, ALP enzymes were significantly increased in all groups, suggesting liver damage. Creatinine levels, indicative of kidney damage, were only significantly increased in rats treated with 15 mg/kg of GNPs repeated doses.

2.5. Histopathological changes

A comprehensive post mortem histological study was then performed to assess any tissue interactions with GNPs. Sections of heart, kidney, liver, small intestine, lung, brain and testis were examined for histopathological changes at 14 and 27 days of GNPs administration (at single or multiple doses of 5 and 15 mg/kg of body weight of rats). The histology photographs of the liver, kidney, heart and small intestine tissues after GNPs exposure of 27 days are shown in Figs. 7 and 8. GNPs at all dosing regimens induced pathological changes after 27 days. Specifically, vacuolation, dilation of central vein and haemorrhage, vacuolation and dilation of central vein, damage of vacuolation, haemorrhage and degeneration of central vein, dilation of epithelial lining and hydropic degeneration oedema were observed in liver tissue. Kidney tissue of the treated groups showed acute vacuolization, dilation of epithelial lining, vacuolation and nucleus degeneration, nucleus damage, necrosis and epithelial degeneration. Heart tissue showed chemodectoma, toxic myocarditis, reddish brown atrophy; yellowish brown pigments suggesting lipofuscin granules as remnants of cell organelles and cytoplasmic material. The brain showed effects of secondary carcinoma, olegodendrocytoma small thin walled blood vessel and crytococcosis. Testicular tissue of treated groups showed spermatogenesis and vacuolation, dilation of germinal layer, degeneration of secondary spermatocytes, damage to the germinal layer and vacuolation. The lung showed damage of vacuolation, degeneration of central vein, inflammation, haemorrhage, d-shaped cells structure, hemosidophroages and lesion. These effects are presumably due to accumulation and low clearance of GNPs in the rat. After the multiple-dose exposure to GNPs, there are some histopathological changes that accumulate around the central veins of the liver. This may be ascribed to the overload of GNP particles in the liver. The histopathological changes of these organs at 14 days in the rats are shown in Supplementary information Figs. 3 and 4. No abnormal clinical signs or death was seen in the all the treated and control groups and all the rats were in good condition at the time of sacrifice.

2.6. Biomarkers of oxidative stress and antioxidant enzymes

The oxidative stress caused by the GNPs in the main organs was measured to examine the possible toxicological pathway. Interestingly, as shown in Fig. 8, the MDA level in the liver of rats treated with a single low dose and multiple low doses (5 mg/kg body weight of rat) remained unchanged. However, the levels

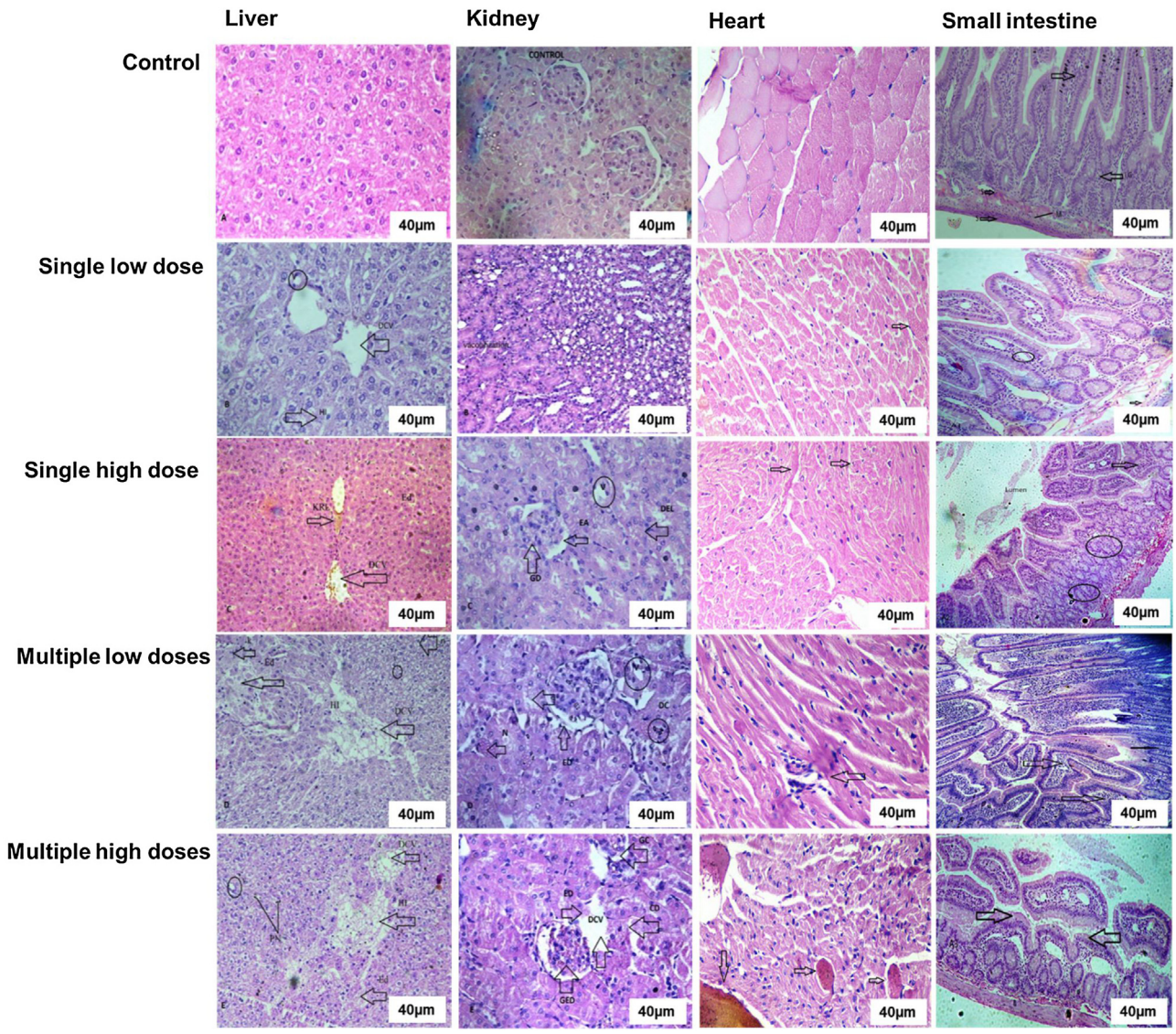

Fig. 7. Representative histopathological changes of the liver, kidney, heart and small intestine of GNPs-exposed and control rats in haemotoxylin-eosin (H&E) stained sections after 27 days. The doses of GNPs were 5 and 15 mg/kg for the single-dose exposure and 5 and 15 mg/kg (every other day, in total fourteen injections) for the multiple-dose exposure. The control group livers showed normal histology while the single low dose group (5 mg/kg) showed vacuolation (circle), dilation of the central vein (DCV indicated by arrow) and haemorrhage (H indicated by arrow). The single high dose group (15 mg/kg) showed haemorrhage (H), vacuolation (V) and dilation of the central vein (DCV) and Karyolysis (K). Multiple low dose group (5 mg/kg) showed the high frequency of vacuolation (circle), haemorrhage (H) and degeneration of central vein (DCV), nuclear damage (N), Karyolysis (K) and epithelial damage (ED). Multiple high dose group (15 mg/kg) in rats exhibited destructive effects on liver haemorrhage (H), massive vacuolation (circle), complete dilation of epithelial lining (ED), dilation of central vein (DCV indicated by arrow) and hydropic degenerative oedema (HDE). Kidney tissues of control group exhibited normal histology. The single low dose group showed acute vacuolization (arrow). The single high dose group caused dilation of epitheliail lining (DEL), vacuolation (circle) and nuclear damage (ND). Kidney tissues of group treated with a multiple low dose exhibited nucleus degeneration (ND), vacuolation (circle), while high dose group showed acute necrosis (N), epithelial degeneration (E) and vacuolization (V). The control group heart showed normal histology of heart muscle tissues and single low dose treated group showed the chemodectoma, an ovoid mass, the tumours were enclosed in a fibrous capsule. The single high dose group indicated toxic myocarditis, and varying degree of damage, ranging from loss of striation to complete necrosis and fragmentation, whereas the multiple low dose group caused acute rheumatism heart, which is the collection of pleomorphic histocytes with large basophilic nuclei having prominent nucleolus which give the cell an 'owl-eye' appearance. While rats treated with a multiple high dose group showed reddish brown atrophy; yellowish brown pigments lipofuscin tends to accumulate in many tissues, the lipofuscin granules were fragments of cell organelles and cytoplasmic material. When the parenchymal cells of an organ exhibited atrophied because of increase age or presence of wasting diseases it may cause the condition of brown atrophy. Histology of control group small intestine showed the normal cell of serosa (s), muscular layer (M), sub mucosa ('S), Intestinal glands (I.G) and Villus (V) and single low dose treated group showed the damage of submucosa and muscular layer (arrow) and enlargement of lacteal (circle). Single high dose treated group showed reduction in villi length (thin arrow), distortion of lamina propria (thick arrow), and intestinal crypts destruction (circle). The multiple low dose treated group exhibited moderate villus atrophy (big arrows) and crypt hyperplasia (small arrow). The multiple high dose group showed total distortion of villi and villus atrophy flat mucosa and no visible microvilli (arrows).

of GSH increased after 27 days of treatment with both single and multiple doses in the liver. GNPs also caused a decrease in the CAT activity in exposed groups with a marked decrease observed in the multiple high dose group (15 mg/kg body weight). Results indicated that under stress, the CAT activity was reduced (Fig. 9).

3. Discussion

Since the isolation of graphene in 2004, research has been conducted to elucidate the potential toxic effects of graphene exposure in *in vitro* and *in vivo* environments. Much research has been carried out on pristine graphene, graphene oxide,

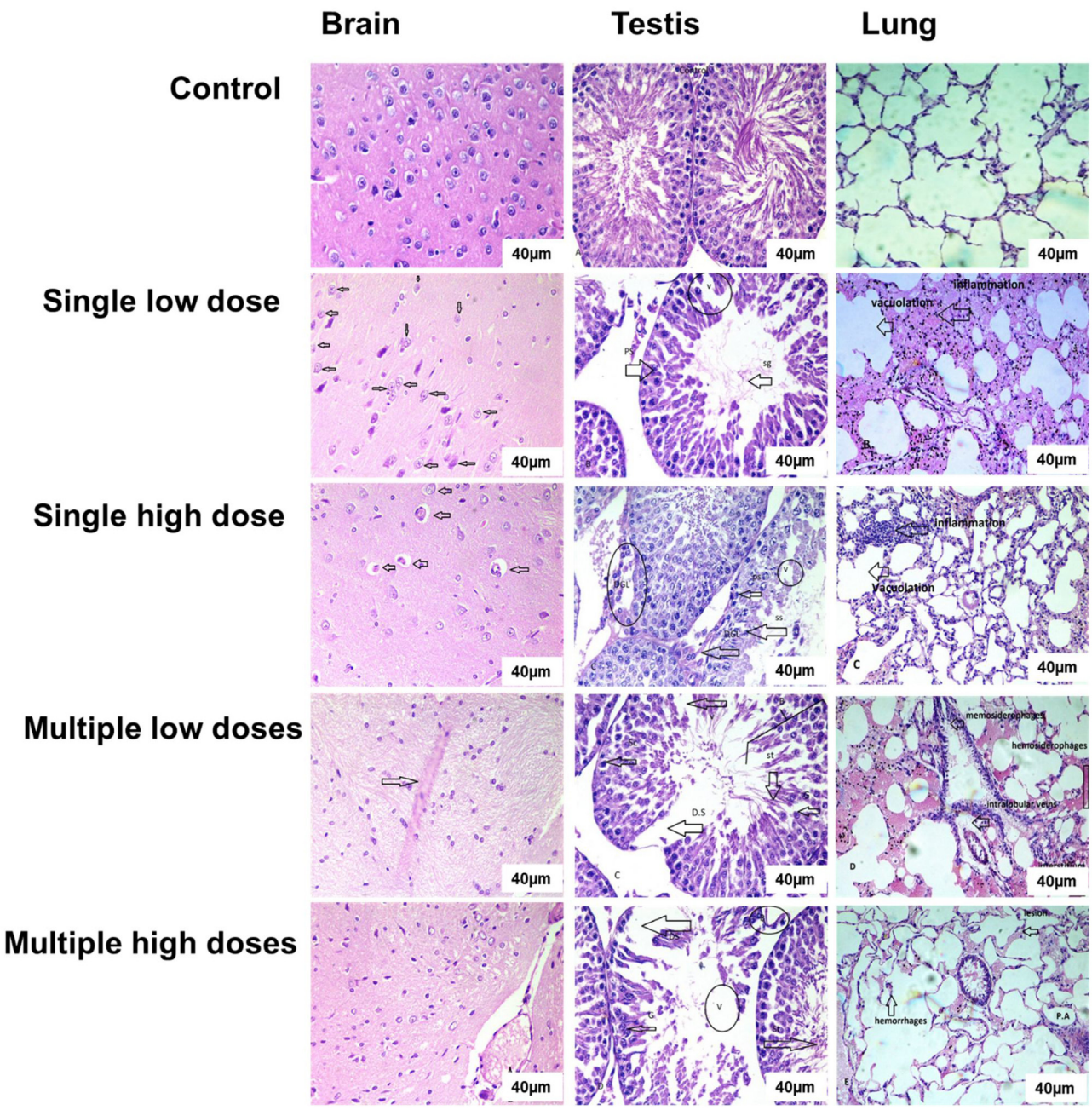

Fig. 8. Representative histopathological changes of the brain, testis and lung of the GNPs-exposed and control rats in haemotoxylin-eosin (H&E) stained sections after 27 days. The doses of GNPs were 5 and 15 mg/kg for the single-dose treatment and 5 and 15 mg/kg (every other day, in total fourteen injections) for the multiple-dose treatments. Control group brain showed normal cells, while rat treated with a single dose (5 mg/kg body weight) exhibited reduced motor neurons and the degenerated sparse neurons (thin arrows). The single high dose treated group exhibited tumours (arrow) and cords of tumour. Rat treated with multiple dose (5 mg/kg body weight) suffered oligodendrocytoma with numerous small thin walled blood vessels (arrow). Rats treated with the multiple high dose group exhibited crytococcosis and a flask shaped depression (arrow). Testicular tissue of the control group of rats exhibited normal histology. Rats treated with a single dose (5 mg/kg body weight) showed spermatogenesis (thin arrow), vacuolation (circle) and primary spermatids (thick arrow). The single high dose treated group showed the dilation of germinal layer (circle), degeneration of secondary spermatocytes (thick large arrow), production of primary spermatids (small arrow), and vacuolation (circle) Rats treated with the multiple low dose group showed dilation of the germinal layer (circle), the degeneration of secondary spermatocytes (thick large arrow), the production of primary spermatids (small arrow), and the vacuolation (circle). The multiple high dose treated group showed vacuolation (circle), damaged basement membrane (B), damaged primary spermatocytes (DS shown by large arrow) and damaged sertoli (st). Control group lung showed normal cells, while rat treated with a single dose (5 mg/kg body weight) exhibited damages of vacuolation, degeneration of central vein and acute inflammation. The single high dose treated group showed damage of vacuolation, haemorrhage and hemosidophroages. Rat treated with multiple dose (5 mg/kg body weight) showed damage of vacuolation, vein and artery damages, disruption, haemorrhage and d-shaped cells structure and hemosidophroages. Rats treated with the multiple high dose group showed damage of vacuolation, vein and artery damage, haemorrhage, d-shaped cells structure, hemosidophroages and lesion.

reduced graphene oxide, graphene quantum dots, and graphene nanoribbons and has showed that these single or few-layered structures are capable of inducing adverse effects in cell lines and animal models [38,39]. These early investigations initiated many pre-clinical toxicity studies on graphene nanostructures designed to inform the potential use of these structures in clinical settings. The results of these studies suggest that graphene nanostructures such as graphene oxide and reduced graphene oxide, have the capacity to induce toxicity in mammals both as a function of their chemistry, by inducing oxidative stress and

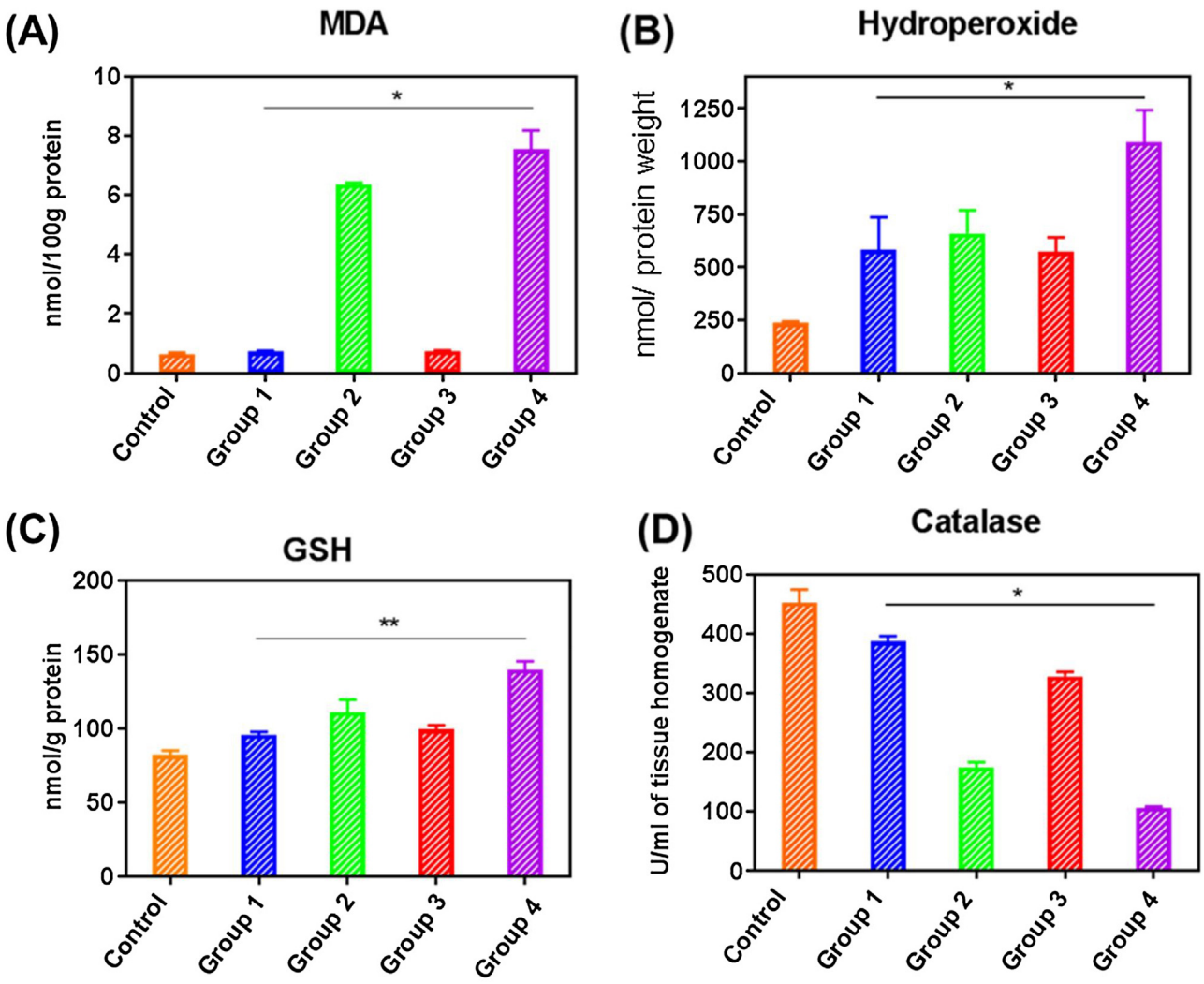

Fig. 9. Biomarkers of oxidative stress results in rats after 27 days of GNPs administration. Rats ($n = 8$ per group) were intraperitoneally injected with single doses of 5 mg/kg body weight (group 1), 15 mg/kg body weight (group 2) and multiple doses of 5 mg/kg body weight (group 3) and 15 mg/kg body weight (group 4). Values are expressed as mean ± standard deviation, for: (A) MDA, (B) hydroperoxide, (C) GSH, and (D) catalase. Data are represented as mean ± SD of three independent experiments. $^{*}p < 0.05$, $^{**}p < 0.01$ vs control. The units of protein weight are per Kg.

lipid peroxidation, and as a result of their aggregation causing physical blockages [40]. Indeed, 3D porous graphene frameworks have shown various effects from acute lethally to sub lethal toxic effects including histological, and oxidative stress responses and, after inhalation exposure in rats, graphene has been found to accumulate in the lung, leading to phagocytosis [30]. However, GNPs, one of the most prominently used derivatives of graphene, e.g. used in DNA sequencing, drug delivery cargos and water treatment, have not been investigated for their potential toxicity [41].

GNPs have different properties from their bulk counterparts based on their size, surface area and porosity. In terms of toxicity a size related increase in surface area can lead to an enhanced dissolution of materials and thus lead to the release of potentially toxic ions and increase in toxic sites. Additionally, due to small pore and sheet sizes, GNPs might be more likely to be retained in cells and organs compared to larger structures. Many studies have shown a size-dependent increase in toxicity as a function of particle size decrease as well as more specific size dependent generation in reactive oxygen species [42]. Although size is an obvious initial determinant of graphene toxicity, many other factors have important contributions to make. Surface charge, stability and aggregation behaviour of GNPs within various exposure environments, are determined both by the physiochemical properties of the surrounding media and the properties of GNPs themselves. A variety of parameters relating to the physiochemical features of GNPs have been shown to influence their toxicity. These parameters are poorly understood, with many studies producing contradictory results, making predicting effects difficult. GNPs can cross cells either para-cellularly or transcellularly, and can travel within the circulatory system and potentially accumulate within tissues and organs [43]. These nanostructures, depending on their composition and physiochemical properties can produce severe damage to cells by inducing oxidative stress [44]. An understanding of the toxicity mechanism is vital to attaining a more uniform understanding and comparison of observed effects.

Here we investigated *in vitro* and *in vivo* toxic effects of GNPs. Our data indicate that GNPs have acute toxicity in SKMES-1 and A549 lung cancer cells cultured *in vitro*. Due to poor solubility and superhydrophobicity, GNPs aggregate and have been reported to bind to proteins on the cell surface and disintegrate membrane integrity [45], and thus measuring cellular membrane integrity is an effective way to detect cell toxicity. The combination of annexin V and PI has been used to discriminate early apoptotic cells from late apoptotic and necrotic ones, based on the translocation of phosphatidylserine from the inner to the outer layer of the plasma

membrane of early apoptotic cells. Annexin V staining is capable of detecting apoptosis, thus revealing this type of cell death. However, PI enters the cell that has lost its membrane integrity, and subsequently flags the cell as late apoptotic/necrotic. Our current study shows that GNPs induce early apoptosis in all cells, however, late apoptosis is only induced at concentrations higher than 250 μg/ml, suggesting that although GNPs at lower concentrations induce flipping of phosphatidylserine on the cell surface membrane, a well-known phenomenon of early apoptotic event, at low concentrations they do not significantly disintegrate the cell membrane. Also, none of the GNPs concentrations tested were found to induce necrosis in SKMES-1 cells, although concentrations higher than 50ug/ml significantly induced necrosis in A549 cells. This may due to the different proteome profile and morphologies of the two cell lines. A number of factors may be involved in the induction of cellular toxicity by GNPs and therefore, testing toxicity in animal models is more physiologically relevant for their real world applications. Hence, we investigated the effect of GNPs at different concentrations in rats, particularly examining toxicity in key organs such as liver, kidney, heart, lung, brain and testis. We also examined measures of oxidative stress in response to graphene which is considered to be a leading cause of cellular toxicity.

Body weight and organ indices are generally considered as biologically relevant to toxicity parameters to investigate the acute exposure of foreign materials in animals [46]. In this study, the first sign of toxicity recorded for the rats given an intraperitoneal injection of GNPs was an observed decrease in body weight at the higher dose. Toxic effects of GNPs on CBC were not observed although there was a slight (6%) reduction in platelet numbers in the 15 mg/kg group. The increased activities of AST, ALT, AMP and creatinine observed after 27 days are indicators of liver and kidney toxicity respectively and appeared in the rats receiving both single and multiple doses of GNPs, compared to control groups. Severe organ damage can increase the activities of ALT and AST and enhanced activity of both are observed when disease processes affect liver cell integrity [47]. Importantly, increased serum ALT activity reflects specific hepatocellular injury [48]. Histopathological alterations were also evident in the liver, where GNPs induced dose- and time-dependent histological alterations of the liver tissues, including congestion, prominent vasodilatation, and vacuolization. Histopathological changes in the liver at 27 days were more pronounced than in rats sacrificed at 14 days following both single and multiple doses of GNPs. The impact of GNPs in these organs could be due to agglomerated states of GNPs which is dependent on the physicochemical synthesis process of GNPs. Minor inflammatory responses were observed in other organs, particularly in the lung which showed isolated areas with granulomatous inflammation. Interestingly, GNPs did not induce any significant histopathological variations in the kidney compared to their control groups, which suggests the rapid clearance of GNPs from the renal tissues. However, the altered creatinine levels observed in rats receiving the highest dose of GNPs does suggest kidney damage. Our data support previous studies that have demonstrated accumulation of graphene nanosheets in the liver, lung, kidneys, and spleen after intraperitoneal, intravenous, or dermal administration [49]. In the present study, the acute intraperitoneal exposure of GNPs at 15 mg/kg for 27 days leads to significant liver damage. This was evidenced by the elevated ALT and ALP serum levels and pathological alterations in the liver. Increased levels of MDA, GSH and lipid peroxidation products were also observed in the liver of GNPs-treated rats. Interestingly, decreased levels of CAT were also found in the liver, suggesting that GNPs reduce the activity of this endogenous antioxidant enzyme, contributing to oxidative stress and hepatocyte damage. This study suggests that more studies are needed to determine the long-term toxicity of porous graphene frameworks via a variety of administration routes to detect any possible serious side effects from such materials.

4. Conclusion

The present study aimed to assess the *in vitro* and *in vivo* interactions of a relatively new derivative of graphene, graphene nanopores (GNPs) in mammalian systems, for the first time and to elucidate the possible mechanism of GNPs toxicity. *In vitro* results showed that GNPs induced early apoptosis in both SKMES-1 and A549 lung cancer cells. However, late apoptosis was only induced at concentrations higher than 250 μg/ml, suggesting that, although GNPs at lower concentrations induced translocation of phosphatidylserine to the cell surface membrane (i.e. early apoptotic event), GNPs do not significantly disintegrate the cell membrane. Subsequently, *in vivo* studies indicated damage in the main organs of rats (liver, kidney, lungs, heart, brain and testis) but the possible fast clearance of GNPs through kidney. We also showed that GNPs induced oxidative stress in the liver. Blood markers remained within normal ranges following treatment. Our results show that changes in liver and kidney functions induced by the treatments were minimal. GNPs caused sub-acute toxicity at our tested doses (5 and 15 mg/kg) to the treated rats in a period of 27 days as evidenced by blood biochemistry, liver and kidney enzyme functions, oxidative stress biomarkers and histological examinations. For the first time, the *in vitro* and *in vivo* toxic effects of a porous graphene nanostructure were investigated. We found time and dose dependent toxicity of GNPs in lung cancer cell lines and rats. These findings will help elucidate how GNPs induce toxicity that may facilitate the modified and biocompatible development of porous graphene-based systems for industrial applications. The potential toxic effects posed by GNPs reveal that the toxicity of other porous derivatives of graphene such as three-dimensional graphene foam, graphene hydrogels, graphene aerogels, porous graphene nanosheets, and other composites must be evaluated to a wide range of cells and animal models to minimize their adverse effects and risks to the off-target living organisms and tissues. The assessment of biosafety and biocompatibility of graphene will certainly have an impact on commercialisation of graphene, and in opening up new gateways for their use in clinical settings. Therefore, long-term, high dose, and careful selection of administration route using different animal models are crucial before seeking any clinical application of this 'wonder material'.

5. Experimental methods

5.1. Synthesis of graphene nanopores

GNPs were synthesized from reduced graphene oxide using our previously reported procedure [21]. Briefly, 150 ml of graphene oxide (1 mg/ml) was mixed with 1.5 ml hydrazine (35%). The reaction mixture was heated at 90–100 °C in an oil bath under magnetic stirring for 12 h until completion. The obtained product was cooled to room temperature, washed with distilled water and filtered to obtain reduced graphene oxide. In the next step, reduced graphene oxide was oven-dried in a vacuum overnight and was thermally heated at 200 °C in Ar for 12 h under a slow ramp rate (3 °C per min). Additional concentrations were prepared in water for further analysis.

5.2. Cell viability

Cell viability was evaluated in A549 and SKMES-1 lung cancer cells. Cells were seeded in 6 well plates at a density of 350,000 per well and cultured in a humidified 5% CO_2 incubator at 37 °C

for 24 h. Cells were treated for 24 h with and without various concentrations (5, 50, 250, 500 and 1000 μg/ml) in culture medium and cells cultured without GNPs were taken as control. Then, cells were trypsinised and centrifuged at 200 g for 5 minutes. Cell pellets were then re-suspended in 100 μl of annexin binding buffer (BioLegend, UK) containing annexin (BioLegend, UK) and propidium iodide (PI) (Sigma–Aldrich, UK), and incubated for 15 minutes in the dark before analysis using flow cytometry.

5.3. Cell apoptosis and necrosis

Cell apoptosis and necrosis were examined using flow cytometry on a Guava flow cytometer (Millipore, Hertfordshire, UK). Signals were detected using Alexa Fluor® 647 which is a bright, far-red–fluorescent dye with excitation ideally suited for the 594 nm and 633 nm laser lines. PI, a yellow-fluorescent dye was excited using the 532 nm laser line. The data were analyzed using Guava 3.1.1 software to determine early and late apoptotic tumour cells. This was done using the following criteria: early and late apoptotic cells were annexin V-positive, PI-negative and annexin V-positive, and PI-positive, respectively. Experiments were repeated 4 times on separate occasions.

5.4. Animals

All animal experiments were performed in compliance with the institutional ethics committee regulations and guidelines on animal welfare (Animal Care and Use Program Guidelines of Government College University), and approved by Government College University, Faisalabad, Pakistan. Sprague-Dawley adult male rats (average age of 6–7 weeks, 230-250 g weight) were obtained from the animal house of Government College University, Faisalabad, housed in groups in ventilated cages under standard lighting conditions and natural day/night cycle after approval from the ethical committee of the institution. They were given free access to water and food and the surrounding humidity and temperature (25 °C ± 2 °C) was controlled. After a period of acclimatization for 7 days, the animals of similar mean initial body weights were randomly divided into five groups, $n = 8$ per group. The body weights of the control group and all the experimental groups were observed and recorded weekly to note weekly changes in body weights. The body weight and behaviour were recorded every day after the first exposure. Organo-somatic index was calculated by the following formula: (weight of the organ (g)/total body weight (g)) 100×. A control group was fed by usual water and food, while the other group was treated with various doses of GNPs (5 mg/kg, 15 mg/kg single and multiple doses) intraperitoneal injections for 27 days. The treatment continued on alternate days for a period of 27 days. Animal exposure schedule was also schematically represented in Supplementary information Fig. 1. At the end of the experimental period, animals were fasted overnight, anaesthetized the next day, by administering ketamine hydrochloride (30 mg/kg body weight) and sacrificed. Blood samples were collected at the start of the experiment and after 27 days of the treatment, from the marginal ear vein, and used for the analysis of complete blood count (CBC), selected serum biochemical parameters, haematology, liver function tests and oxidative stress enzymes.

5.5. Complete blood count (CBC) and clinical biochemistry panel analysis

Haematological parameters: Red blood cell count (RBC); lymphocytosis (LYM %); mid-range absolute count (MID); total % of granulocytes GRA; haemoglobin (HBGL); mean corpuscular haemoglobin (MCH); mean corpuscular haemoglobin concentration (MCHC); mean corpuscular volume (MCV); hematocrit (HCT); red cell distribution width (RDW); platelet count (PLT); mean platelet component (MPC); large platelet concentration ration (LPCR); and white blood cell count (WBC), were analyzed in blood samples using a Hitachi 902 automatic analyser (Japan). Blood samples were collected in heparinised tubes, and plasma was separated by centrifugation at 2000 × g for 10 min. The livers were collected, weighed using a Sartorius weighing balance and separately immersed in fixative for further histological processing (by the haematoxylin-eosin staining method).

5.6. Liver and kidney function analysis

To evaluate the liver function, the levels of alanine aminotransaminase (ALT), aspartate aminotransferase (AST) and alkaline phosphatase (ALP) were determined. To evaluate kidney function, the levels of creatinine were measured. Concentrations of these enzymes were determined using commercial reagent kits (CHEMELEX, S.A Pol. Ind, Barcelona, Spain) and an autoanalyser system (Hitachi Ltd., Tokyo, Japan) following the International Federation of Clinical Chemistry (IFCC) method [50].

5.7. Histological analysis

The harvested heart, liver, spleen, kidney, lung, brain, intestine and testis were fixed with 4% paraformaldehyde for 5 hours and then dehydrated and processed for histology. Sections (6 μm) were cut from paraffin blocks using a Reichert microtome and stained with eosin (cytoplasm staining). The stained slides were examined by light microscopy through a 20× or 40× objective lens. A histological analysis of vital organs was performed to determine whether or not the GNPs or the degradation of GNPs caused tissue damage and/or any pathologic impacts such as inflammation or necrosis.

5.8. Oxidative stress biomarkers and antioxidant enzymes

The activities of antioxidant enzymes, i.e. catalase activity, superoxide dismutase activity, glutathione-S-transferase activity and lipid peroxidation, were measured. To determine these parameters in the liver, the liver was quickly removed, washed in ice-cold isotonic saline solution and blotted individually on ash-free filter paper. The tissues were then homogenized in 0.1 M Tris–HCl buffer, pH 7.4, using a Potter-Elvejham homogenizer at 4 °C with a diluting factor of 4, the crude tissue homogenate was then centrifuged at 10,000 rpm for 15 min at 4 °C and the supernatant was kept at −20 °C for the estimation of enzyme activity analysis [51]. The concentration of lipid peroxidation end product (MDA) in the liver tissue homogenate (50 mg tissues in 1.5 ml of 0.1 M tris–HCl buffer, pH 7.4) was determined by the method reported by Okhawa et al. [52]. Briefly, the reaction mixture contained 0.2 ml of 10% (w/v) tissue homogenate, 0.2 ml of 8.1% sodium dodecyl sulfate, 1.5 ml of 20% acetic acid and 1.5 ml of 0.8% aqueous solution of thiobarbutaric acid (TBA). The pH of 20% acetic acid was pre-adjusted with 1 M NaOH to 3.5. The mixture was made up to 4 ml with distilled water and heated at 95 °C for 1 h, in a water bath using glass ball as a condenser. After cooling in tap water, 1 ml of distilled water and 5 ml of mixture of n-butanol and pyridine (15:1) were added and mixture was shaken vigorously on a vortex mixer (Bio Vortex, peQ Lab, UK). After centrifugation at 4000 rpm for 10 min the absorbance of the upper organic layer was read at 532 nm. Tetramethoxy-propane (TMP) was used as an external standard, and the level of lipid peroxidation was expressed as nmol of MDA. The values of lipid peroxidation were expressed in nmol/ protein weight of tissues. The reduced glutathione (GSH) was estimated according to the method described in ref [53]; catalase [54]; and lipid hydroperoxides [55]. The estimation of lipid hydroperoxides was carried out following the method reported by Jiang et al. [55],

in which 0.1 ml of 10% (w/v) tissue homogenate was treated with 0.9 ml of fox reagent (88 mg of butylated hydroxytoluene, 7.6 mg of xylenol orange and 9.8 mg of ammonium iron sulfate which were added to 90 ml methanol and 10 ml 250 mM sulphuric acid) and incubated at 37 °C for 30 min. The colour developed was then read at 560 nm and the lipid hydroperoxides were expressed as mM/g of tissues.

5.9. Statistical analysis

The data were statistically analyzed in GraphPad Prism 5.04 to determine the GNPs treatment effects on various parameters of cell count, body weight, liver and kidney function tests, complete blood count and oxidative stress biomarkers. $p < 0.05$ was considered as statistically significant. Results were presented as the mean ± standard deviation (SD).

Acknowledgement

This work was supported by EPSRC Centre for Doctoral Training in Metamaterials, XM^2 [Grant no. EP/L015331/1] the University Of Exeter EX4, United Kingdom and FORCE Cancer Charity [Grant No. 50703] United Kingdom.Supplementary data

Supplementary data associated with this article can be found, in the online version, at doi:10.1016/j.apmt.2018.07.005.

References

[1] K. Kostarelos, K.S. Novoselov, Graphene devices for life, Nat. Nanotechnol. 9 (10) (2014) 744–745.
[2] K. Kostarelos, K.S. Novoselov, Exploring the interface of graphene and biology, Science 344 (6181) (2014) 261–263.
[3] M. Fojtů, W.Z. Teo, M. Pumera, Environmental impact and potential health risks of 2D nanomaterials, Environ. Sci.: Nano 4 (8) (2017) 1617–1633.
[4] Q. Wan, Q. Huang, M. Liu, D. Xu, H. Huang, X. Zhang, Y. Wei, Aggregation-induced emission active luminescent polymeric nanoparticles: non-covalent fabrication methodologies and biomedical applications, Appl. Mater. Today 9 (2017) 145–160.
[5] T.A. Tabish, S. Zhang, P.G. Winyard, Developing the next generation of graphene-based platforms for cancer therapeutics: the potential role of reactive oxygen species, Redox Biol. 15 (2018) 34–40.
[6] N. Li, Q. Zhang, S. Gao, Q. Song, R. Huang, L. Wang, G. Cheng, Three-dimensional graphene foam as a biocompatible and conductive scaffold for neural stem cells, Sci. Rep. 3 (2013) 1604.
[7] G.F. Schneider, C. Dekker, DNA sequencing with nanopores, Nat. Biotechnol. 30 (4) (2012) 326–328.
[8] G.F. Schneider, S.W. Kowalczyk, V.E. Calado, G. Pandraud, H.W. Zandbergen, L.M. Vandersypen, C. Dekker, DNA translocation through graphene nanopores, Nano Lett. 10 (8) (2010) 3163–3167.
[9] C.A. Merchant, K. Healy, M. Wanunu, V. Ray, N. Peterman, J. Bartel, M. Drndic, DNA translocation through graphene nanopores, Nano Lett. 10 (8) (2010) 2915–2921.
[10] S.P. Surwade, S.N. Smirnov, I.V. Vlassiouk, R.R. Unocic, G.M. Veith, S. Dai, S.M. Mahurin, Water desalination using nanoporous single-layer graphene, Nat. Nanotechnol. 10 (5) (2015) 459–464.
[11] D. Cohen-Tanugi, J.C. Grossman, Water desalination across nanoporous graphene, Nano Lett. 12 (7) (2012) 3602–3608.
[12] S. Garaj, W. Hubbard, A. Reina, J. Kong, D. Branton, J.A. Golovchenko, Graphene as a subnanometre trans-electrode membrane, Nature 467 (7312) (2010) 190–193.
[13] D.P. Linklater, V.A. Baulin, S. Juodkazis, E.P. Ivanova, Mechano-bactericidal mechanism of graphene nanomaterials, Interface Focus 8 (3) (2018) 20170060.
[14] R.K. Matharu, L. Ciric, M. Edirisinghe, Nanocomposites: suitable alternatives as antimicrobial agents, Nanotechnology 29 (28) (2018) 282001.
[15] R.K. Matharu, H. Porwal, L. Ciric, M. Edirisinghe, The effect of graphene–poly (methyl methacrylate) fibres on microbial growth, Interface Focus 8 (3) (2018) 20170058.
[16] T.A. Tabish, L. Lin, M. Ali, F. Jabeen, R. Iqbal, D.W. Horsell, P.G. Winyard, S. Zhang, Investigating the bioavailability of graphene quantum dots in lung tissues via Fourier transform infrared spectroscopy, Interface Focus 8 (3) (2018) 20170054.
[17] Z. Lin, G.H. Waller, Y. Liu, M. Liu, C.P. Wong, Simple preparation of nanoporous few-layer nitrogen-doped graphene for use as an efficient electrocatalyst for oxygen reduction and oxygen evolution reactions, Carbon 53 (2013) 130.
[18] L. Shi, L. Wang, J. Chen, J. Chen, L. Ren, X. Shi, Y. Wang, Modifying graphene oxide with short peptide via click chemistry for biomedical applications, Appl. Mater. Today 5 (2016) 111–117.
[19] S. Reyntjens, R. Puers, A review of focused ion beam applications in microsystem technology, J. Micromech. Microeng. 11 (4) (2001) 287.
[20] W. Yuan, J. Chen, G. Shi, Nanoporous graphene materials, Mater. Today 17 (2) (2014) 77–85.
[21] T.A. Tabish, F.A. Memon, D.E. Gomez, D.W. Horsell, S. Zhang, A facile synthesis of porous graphene for efficient water and wastewater treatment, Sci. Rep. 8 (2018).
[22] R. Augustine, A.P. Mathew, A. Sosnik, Metal oxide nanoparticles as versatile therapeutic agents modulating cell signaling pathways: linking nanotechnology with molecular medicine, Appl. Mater. Today 7 (2017) 91–103.
[23] K. Habiba, D.P. Bracho-Rincon, J.A. Gonzalez-Feliciano, J.C. Villalobos-Santos, V.I. Makarov, D. Ortiz, . . ., G. Morell, Synergistic antibacterial activity of PEGylated silver–graphene quantum dots nanocomposites, Appl. Mater. Today 1 (2) (2015) 80–87.
[24] C. Guo, L. Sun, H. Cai, Z. Duan, S. Zhang, Q. Gong, Z. Gu, Gadolinium-labeled biodegradable dendron–hyaluronic acid hybrid and its subsequent application as a safe and efficient magnetic resonance imaging contrast agent, ACS Appl. Mater. Interfaces 9 (28) (2017) 23508–23519.
[25] Q. Luo, X. Xiao, X. Dai, Z. Duan, D. Pan, H. Zhu, Q. Gong, Cross-linked and biodegradable polymeric system as a safe magnetic resonance imaging contrast agent, ACS Appl. Mater. Interfaces 10 (2) (2018) 1575–1588.
[26] F. Perreault, A.F. De Faria, M. Elimelech, Environmental applications of graphene-based nanomaterials, Chem. Soc. Rev. 44 (16) (2015) 5861–5896.
[27] C. Bussy, H. Ali-Boucetta, K. Kostarelos, Safety considerations for graphene: lessons learnt from carbon nanotubes, Acc. Chem. Res. 46 (3) (2012) 692–701.
[28] B. Zhang, H. Ni, R. Chen, T. Zhang, X. Li, W. Zhan, Y. Xu, Cytotoxicity effects of three-dimensional graphene in NIH-3T3 fibroblasts, RSC Adv. 6 (51) (2016) 45093–45102.
[29] T.A. Tabish, S. Chabi, M. Ali, Y. Xia, F. Jabeen, S. Zhang, Tracing the bioavailability of three-dimensional graphene foam in biological tissues, Materials 10 (4) (2017) 336.
[30] A. Schinwald, F.A. Murphy, A. Jones, W. MacNee, K. Donaldson, Graphene-based nanoplatelets: a new risk to the respiratory system as a consequence of their unusual aerodynamic properties, ACS Nano 6 (1) (2012) 736–746.
[31] H. Cai, X. Wang, H. Zhang, L. Sun, D. Pan, Q. Gong, K. Luo, Enzyme-sensitive biodegradable and multifunctional polymeric conjugate as theranostic nanomedicine, Appl. Mater. Today 11 (2018) 207–218.
[32] L. Mao, M. Hu, B. Pan, Y. Xie, E.J. Petersen, Biodistribution and toxicity of radio-labeled few layer graphene in mice after intratracheal instillation, Particle Fibre Toxicol. 13 (1) (2015) 7.
[33] M. Pelin, L. Fusco, V. León, C. Martín, A. Criado, S. Sosa, M. Prato, Differential cytotoxic effects of graphene and graphene oxide on skin keratinocytes, Sci. Rep. 7 (2017) 40572.
[34] M. Wojtoniszak, X. Chen, R.J. Kalenczuk, A. Wajda, J. Łapczuk, M. Kurzewski, E. Borowiak-Palen, Synthesis, dispersion, and cytocompatibility of graphene oxide and reduced graphene oxide, Colloids Surf. B: Biointerfaces 89 (2012) 79–85.
[35] T.A. Tabish, M.Z.I. Pranjol, H. Hayat, A.A. Rahat, T.M. Abdullah, J.L. Whatmore, S. Zhang, In vitro toxic effects of reduced graphene oxide nanosheets on lung cancer cells, Nanotechnology 28 (50) (2017) 504001.
[36] Y. Ma, H. Shen, X. Tu, Z. Zhang, Assessing in vivo toxicity of graphene materials: current methods and future outlook, Nanomedicine 9 (10) (2014) 1565–1580.
[37] Wilding, L. Jennifer, F. Walter, Bodmer, Cancer cell lines for drug discovery and development, Cancer Res. 74 (9) (2014) 2377–2384.
[38] Y. Chong, Y. Ma, H. Shen, X. Tu, X. Zhou, J. Xu, Z. Zhang, The in vitro and in vivo toxicity of graphene quantum dots, Biomaterials 35 (19) (2014) 5041–5048.
[39] D.A. Jasim, H. Boutin, M. Fairclough, C. Ménard-Moyon, C. Prenant, A. Bianco, K. Kostarelos, Thickness of functionalized graphene oxide sheets plays critical role in tissue accumulation and urinary excretion: a pilot PET/CT study, Appl. Mater. Today 4 (2016) 24–30.
[40] D.D. Chronopoulos, A. Bakandritsos, M. Pykal, R. Zbořil, M. Otyepka, Chemistry, properties, and applications of fluorographene, Appl. Mater. Today 9 (2017) 60–70.
[41] C. Bussy, D. Jasim, N. Lozano, D. Terry, K. Kostarelos, The current graphene safety landscape – a literature mining exercise, Nanoscale 7 (15) (2015) 6432–6435.
[42] A. Montagner, S. Bosi, E. Tenori, M. Bidussi, A.A. Alshatwi, M. Tretiach, Z. Syrgiannis, Ecotoxicological effects of graphene-based materials, 2D Materials 4 (1) (2016) 012001.
[43] R.X. Wu, X.Y. Xu, J. Wang, X.T. He, H.H. Sun, F.M. Chen, Biomaterials for endogenous regenerative medicine: coaxing stem cell homing and beyond, Appl. Mater. Today 11 (2018) 144–165.
[44] N.F. Rosli, N.M. Latiff, Z. Sofer, A.C. Fisher, M. Pumera, In vitro cytotoxicity of covalently protected layered molybdenum disulfide, Appl. Mater. Today 11 (2018) 200–206.
[45] S. Liu, T.H. Zeng, M. Hofmann, E. Burcombe, J. Wei, R. Jiang, Y. Chen, Antibacterial activity of graphite, graphite oxide, graphene oxide, and reduced graphene oxide: membrane and oxidative stress, ACS Nano 5 (9) (2011) 6971–6980.

[46] S. Reagan-Shaw, M. Nihal, N. Ahmad, Dose translation from animal to human studies revisited, FASEB J. 22 (3) (2008) 659–661.
[47] S.K. Ramaiah, A toxicologist guide to the diagnostic interpretation of hepatic biochemical parameters, Food Chem. Toxicol. 45 (9) (2007) 1551–1557.
[48] J. Ozer, M. Ratner, M. Shaw, W. Bailey, S. Schomaker, The current state of serum biomarkers of hepatotoxicity, Toxicology 245 (3) (2008) 194–205.
[49] X. Guo, N. Mei, Assessment of the toxic potential of graphene family nanomaterials, J. Food Drug Anal. 22 (1) (2014) 105–115.
[50] B. Lefrere, A. Servonnet, F. Ceppa, F. Dorandeu, H. Delacour, Use of IFCC guidelines to verify acetylcholinesterase reference interval in adults determined with ChE check mobile testing system, Clinical Chemistry and Laboratory Medicine (CCLM), 2017.
[51] M.A. Dkhil, R. Zrieq, S. Al-Quraishy, A.E. Abdel Moneim, Selenium nanoparticles attenuate oxidative stress and testicular damage in streptozotocin-induced diabetic rats, Molecules 21 (11) (2016) 1517.
[52] H. Ohkawa, N. Ohishi, K. Yagi, Assay for lipid peroxides in animal tissues by thiobarbituric acid reaction, Anal. Biochem. 95 (2) (1979) 351–358.
[53] D.J. Jollow, J.R. Mitchell, N. Zampaglione, J.R. Gillete, Bromobenzene induced liver necrosis. Protective role of glutathione and evidence for 3,4-bromobenzeneoxide as the hepatotoxic metabolite, Pharmacology 11 (1974) 151–169.
[54] H. Aebi, Catalase, in: L. Packer (Ed.), Methods in Enzymology, 105, Academic Press, Orlando, FL, 1984, pp. 121–126.
[55] Z.Y. Jiang, J.V. Hunt, S.P. Wolff, Ferrous ion oxidation in the presence of xylenol orange for detection of lipid hydroperoxide in low density lipoprotein, Anal. Biochem. 202 (2) (1992) 384–389.